How does yawed inflow affect the performance of ducted wind turbines?

Dighe, Vinit; Suri, Dhruv; Avallone, Francesco; van Bussel, Gerard

Important note
To cite this publication, please use the final published version (if applicable).
Please check the document version above.

How does yawed inflow affect the performance of ducted wind turbines?

V.V. Dighe*

Delft University of Technology, Delft, Netherlands.

D. Suri [†]

Manipal Institute of Technology, Karnataka, India.

F. Avallone [‡], G.J.W. van Bussel [§]

Delft University of Technology, Delft, Netherlands.

Ducted Wind Turbines (DWTs) are used for energy harvesting in urban areas where the flow is non-uniform in comparison to the free-field because of the presence of buildings or other surface discontinuities. For this reason, the aerodynamic performance and far-field noise of DWTs in yawed inflow conditions must be characterized. Both the aerodynamic and the acoustic fields are dependent on the geometry of the duct. In this study, the effect of the duct geometry is analysed with high fidelity numerical simulations carried out with the lattice-Boltzmann method.

Nomenclature

c	Duct chord length [m]
c_p	Pressure coefficient [-]
C_P	Power coefficient [-]
$C_{T,duct}$	Duct thrust coefficient [-]
D_{in}	Duct inlet diameter [m]
D_{out}	Duct outlet diameter [m]
D_{rot}	Turbine diameter [m]
D_{th}	Duct throat diameter [m]
t	Maximum thickness of the duct profile [%c]
U_∞	Free-stream velocity [m/s]
x	Variable value vector parallel to the free-stream direction [-]
y	Variable value vector normal to the free-stream direction [-]
AD	Actuator disk
DWT	Ducted wind turbine
$HAWT$	Horizontal axis wind turbine
$LCOE$	Levelized cost of electricity

I.   Introduction

GLOBAL energy demand is expected to more than double by 2050 owing to the growth in population and development of economies.[1] Wind energy is emerging as an alternative renewable source for energy production. Presently, wind turbines are typically installed away from the populated areas because of visual

---

*PhD Researcher, Wind Energy Research Group, Member AIAA

[†]Undergraduate Student, Department of Aeronautical and Automobile Engineering, Student Member AIAA

[‡]Assistant Professor, Wind Energy Research Group, Member AIAA

[§]Professor, Wind Energy Research Group, Member AIAA

American Institute of Aeronautics and Astronautics

and noise regulations. This necessitates the transfer of electricity via grids over larger distances, which increases the levelized cost of electricity.

A possible technological solution to extract wind energy in urban areas is represented by Ducted Wind Turbines (DWTs). DWTs increase the energy extraction with respect to conventional horizontal axis wind turbines (HAWTs) for a given turbine radius and free-stream velocity.[2] DWTs are constituted of a turbine and a duct (also named as diffuser or shroud); the role of the latter is to increase the flow rate through the turbine relative to a similar turbine operating in the open atmosphere, thereby increasing the generated power. However, because of the high turbulent and non-uniform flow in urban areas, DWTs are expected to operate under yawed inflow conditions, but this aspect has not been widely studied in the literature.

Igra[4] studied experimentally the effects of yawed flow on the aerodynamic performance of DWTs. Eight geometries, with different duct cross-sections and actuator disc (AD) thrust coefficients, were investigated using simplified duct-AD models. He found that the aerodynamic performance of the duct-AD system increases with increasing yaw angle up to a specific angle; thereafter any further increase of yaw angle results in performance drop. On the other hand, using a slotted duct, the performance of the system decreases with increasing yaw angle. On the same line, Phillips et al.[5] combined experimental and computational analysis to study DWTs in yawed flow. Conversely, they concluded that the power increase for a DWT in yawed flow can only be achieved with a slotted duct design, with the added mass flow of air through the slot increasing the boundary layer flow control and preventing flow separation over the inner surface of the duct under severe yaw misalignment.

The above literature, due to the contrasting nature of the conclusions, lacks clarity on the aerodynamics of DWTs in yawed flow, and particularly on the effects of the duct geometry on the aerodynamic performances. In addition, the simplifications caused by the use of the AD do not allow a coherent analysis of the unsteady three-dimensional flow within the duct, which further affects the aerodynamic and aeroacoustic performance of a DWT.

The goal of the present paper is to characterize the effects of yawed inflow on the aerodynamic and aeroacoustic performance of DWTs. This is performed using computational fluid dynamics (CFD). Two reference DWT geometries are selected. Simulations are performed using Lattice-Boltzmann Very-Large Eddy Simulations (LB-VLES).

II.   Numerical approach

A.   Lattice Boltzmann solver

The CFD solver Simulia PowerFLOW® based on the lattice-Boltzmann method (LBM) is used to calculate the unsteady flow around the DWT models. The solver has been validated for aerodynamic and aeroacosutic analysis for a similar class of problems.[9, 10]

The software solves the LB equations for a finite number of directions. LB equations, by nature, are explicit, transient and compressible. For a detailed description, the reader can refer to Chen et al.[11] and Succi.[12] For an incompressible fluid in isothermal conditions, the Navier Stokes equations can be derived from the LB equations.[13] Statistically, the LB equations describe the particle motion at a position x in the i-th direction at time t. The macroscopic flow variables, such as density and velocity, are determined by taking summation over the set of discrete directions of the particle distribution function. The particle distribution function $\Omega(f)$ is solved by means of the Boltzmann equation on a mesh composed of cubic volumetric elements (voxels) and surface elements (surfels), known as lattice. A VLES model is implemented to take into account the unresolved scales of turbulence. A two equation $k - \epsilon$ Renormalization Group (RNG) is used to compute the turbulent relaxation time that is added to the viscous relaxation time.

A pressure-gradient-extended wall-model is used to approximate the no-slip boundary condition on solid walls.[14] The model is based on the extension of the generalized law-of-the-wall model[15] to take into account the effect of pressure gradient, given by the following analytical expression:

$$u^+ = \frac{1}{k} ln(\frac{y^+}{A}) + B \tag{1}$$

where u^+ and y^+ are the boundary-layer velocity and the non-dimensional wall distance, respectively, $k = 0.41$ is the von Karman constant and $B = 5.2$ is the log-law constant. A is a function of pressure gradient. It captures the physical consequence that the velocity profile slows down and so expands, due to the presence of the pressure gradient, at least at the early stage of the development. The expression for A is:

American Institute of Aeronautics and Astronautics

$$A = 1 + \frac{f \left| \frac{dp}{ds} \right|}{\tau_w}, \quad \hat{u}_s \cdot \frac{dp}{ds} = 0, \tag{2}$$

$$A = 1, \quad \text{otherwise.} \tag{3}$$

In the equations, τ_w is the wall shear stress, $\frac{dp}{ds}$ is the stream-wise pressure gradient, $\hat{u}_s$ is the unit vector of the local slip velocity and f is the length scale equal to the size the unresolved near-wall region. These equations are iteratively solved from the first mesh cell close to the wall in order to specify the boundary conditions of the turbulence model. For this purpose, a slip algorithm,[16] obtained as generalization of a bounce-back and specular reflection process, is used.

The transient nature of the LB-VLES solutions allow the extraction of acoustic pressure in the near-field up to a cut-off frequency corresponding to approximately 15 voxels per acoustic wavelength. The acoustic pressure in the far-field is computed by using the Ffowcs Williams-Hawkings (FWH) analogy.[17] The formulation 1A developed by Farrasat with advanced-time solution,[18] extended to a convective wave equation, is used in this study. Unsteady pressure fluctuations, used to compute far-field sound, are recorded on the surface of the DWT model.

B.   Numerical setup

Two duct geometries with different longitudinal airfoil cross section (named as DonQi® and DonQi D5) are chosen. The selection is based on the existing study conducted by the authors.[6] For both the duct geometries, the diameter is equal to $D_{in} = 1.74$ m at the inlet, $D_{th} = 1.54$ m at the throat and $D_{out} = 2$ m at the exit, while the duct chord length equals to $c = 1$ m. The suction side of both the duct geometries are identical. For the duct model DonQi D5, the pressure side of the duct is bent in the chord-wise direction resulting in a maximum thickness to chord ratio $\frac{t}{c} = 10.36\%$; this ratio is 20.60% for duct model DonQi®. The turbine diameter is equal to $D_{rot} = 1.5$ m, and comprises of three blades with a NACA 2207 airfoil cross-section. The blades are connected to a hub (upstream) and a nacelle (downstream).
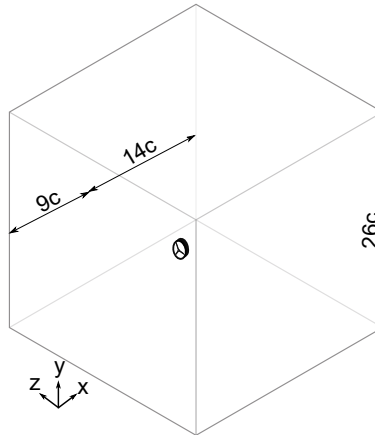

Figure 1: Computational domain used for the LB-VLES simulations. The length are indicated in terms of duct chord length c (representative, not to scale).

The simulation domain is a rectangular box equal to $23c$ in the free-stream direction x, and $26c$ in the y direction perpendicular to the flow; see Figure 1. The DWT model is located $9c$ downstream of the inlet. Free-stream boundary conditions are applied at the inlet while pressure outlet boundary conditions are applied at the outlet. The side walls are defined using slip boundary conditions. In total, approximately 284 million voxels and 52 million of surfels are used to discretize a single case. A total of 11 mesh refinement regions, named as VR, with resolution factor equal to 2 are employed. The calculation time is 1.42 seconds (9 revolutions) requiring 7200 CPU hrs/rev on a Linux Xeon E5-2690 2.9 GHz platform. Additional details on the numerical implementation are given by Avallone et al.[7]

American Institute of Aeronautics and Astronautics

C. Numerical solution verification and validation

First, a mesh independence study is performed for the DonQi[®] DWT model in non-yawed inflow condition by uniformly increasing the resolution of each VR. Three resolution cases, corresponding to the smallest voxel size equal to 1200 (coarse), 1800 (medium) and 2400 (fine) voxels per duct chord, are studied. The total thrust force coefficient C_T for the DWT model is taken as reference for the convergence analysis, given by:

$$C_T = \frac{T}{\frac{1}{2}\rho U_\infty^2 S_{exit}}.$$ (4)

where T is the total thrust force, i.e. the axial force, generated by the DWT model and S_{exit} is the duct exit surface area equal to πR_{exit}^2.

The results of the mesh independence study are shown in Table 1. Solution convergence is reached for the medium VR, when the observed deviations between the converged values are less than 0.5%. The medium VR mesh is then used in the rest of the paper.

Table 1: Voxels statistics for mesh independence study of the DWT models.

	Coarse	Medium	Fine	Experiments
Number of voxels	1.46×10^6	2.67×10^6	4.33×10^6	
DonQi[®] C_T	0.612	0.703	0.706	0.689

As further validation of the numerical approach, numerical results are compared with the experimental ones reported by Ten Hoopen.[19] He investigated experimentally the DonQi[®] DWT model in non-yawed inflow condition. Experiments were conducted in the closed-loop open-jet (OJF) wind tunnel facility at the Delft University of Technology. The total thrust force exerted by the DonQi[®] DWT model was measured using an axial force balance system. The C_T calculated from the wind tunnel measurements is 0.689 while by CFD it is 0.703; see Table 1. The numerical and experimental results differ by 2%, which is within the experimental uncertainty.

III. Results and discussion

In this section, two DWT geometries operating under two different inflow conditions are studied, corresponding to: (a) DonQi[®] model with 0° yaw (b) DonQi[®] model with 7.5° yaw (c) DonQi D5[®] model with 0° yaw and (d) DonQi D5[®] model with 7.5° yaw. The specific choice of yaw angle selection follows a previous study.[8]

A. Flow-field analysis

The instantaneous flow-fields around the two DWT models, both in non-yawed and yawed inflow conditions, are shown in Figure 2 using the λ2-criterion colored with the velocity magnitude.[20] λ2 isosurfaces highlights the presence of turbulent structures in the flow. DonQi[®] model at 0° yaw (Figure 2 (a)) show coherent vortices convecting inside of the duct. These vortices follow a helicoidal path due to turbine rotation. For DonQi D5 DWT model, however, large coherent structures are also present on the pressure side of the duct because of the larger camber with respect to the DonQi[®] model, see Figure 2 (c).

By introducing a yaw angle, as in Figures 2 (b) and (d), the flow-fields, for both configurations, show differences in the turbulent flow structures convecting over the inner walls of the duct. A major difference between the two configurations is that, for the DonQi[®] model, the tip vortex is generated at the turbine plane and interact with the duct surface at downstream locations where it breaks in smaller structures. Differently, for the DonQi D5 model, as for the case with zero yaw angle, the tip vortex breaks at the turbine plane. For this case, the flow is richer of turbulent flow structures, and it decelerates just downstream of the turbine plane as visible from the blue contour representing normalized streamwise velocity component. For this particular case, the yawed inflow causes an early breakdown of the main vortex into smaller structures at the pressure side of the duct.
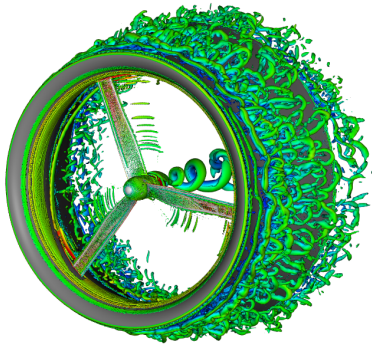
To better show the aerodynamic interactions between the duct and the turbine, 2D visualization in the x-y plane of the instantaneous flow-fields are shown in Figure 3. Contours are plotted on a cross-section
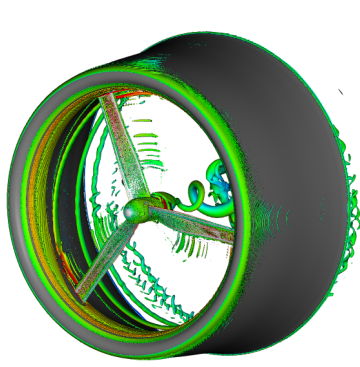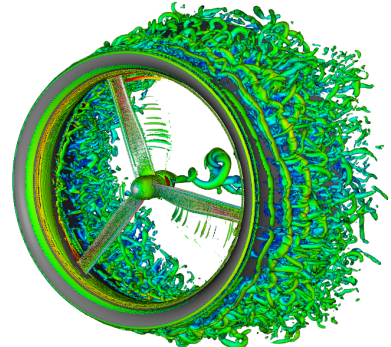
American Institute of Aeronautics and Astronautics

(a) DonQi® model with 0° yaw
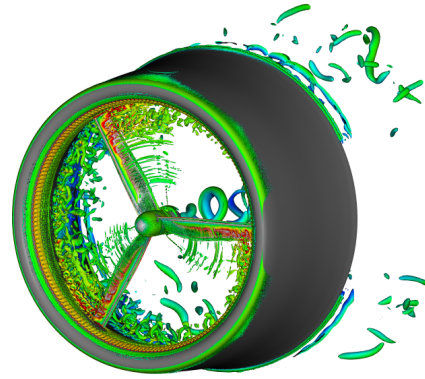
(b) DonQi® model with 7.5° yaw

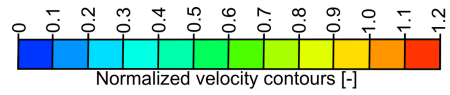(c) DonQi D5® model with 0° yaw

(d) DonQi D5® model with 7.5° yaw

Figure 2: Visualization of the instantaneous flow field for the two DWT configurations under two different operating conditions. Iso-surface of the $\lambda 2$ criterion colored with the velocity magnitude.

plane, thus allowing a better interpretation. For the non-yawed case, the flow is attached upto 95% of the duct chord for the DonQi® model, conversely, inner duct wall flow separation is visible starting from 80% of duct chord for the DonQi D5 model. On the other hand, flow separation increases both on the duct wall and higher velocity fluctuations is observed at the root region of the blade for the DonQi® model at 7.5° yaw (Figure 3 (b)). These velocity fluctuations in the near wake resembles the vortex dynamics breakdown for HAWTs in yaw, thus reducing the overall thrust generated by the turbine blades. From a deeper look, flow remains attached on the pressure side of the duct to a larger extent for the DonQi D5 model under 7.5° yaw, see Figure 3 (d). Also, the effect of the increase of the velocity at the turbine plane starts to appear and the thrust generated by the turbine increases. As a matter of fact, for the DonQi D5 model in yawed inflow (Figure 3 (d)), the separation location within the duct weakly changes with respect to the non-yawed configuration.

(a) DonQi® model with 0° yaw

(b) DonQi® model with 7.5° yaw

(c) DonQi D5® model with 0° yaw

(d) DonQi D5® model with 7.5° yaw

Normalized velocity contours [-]
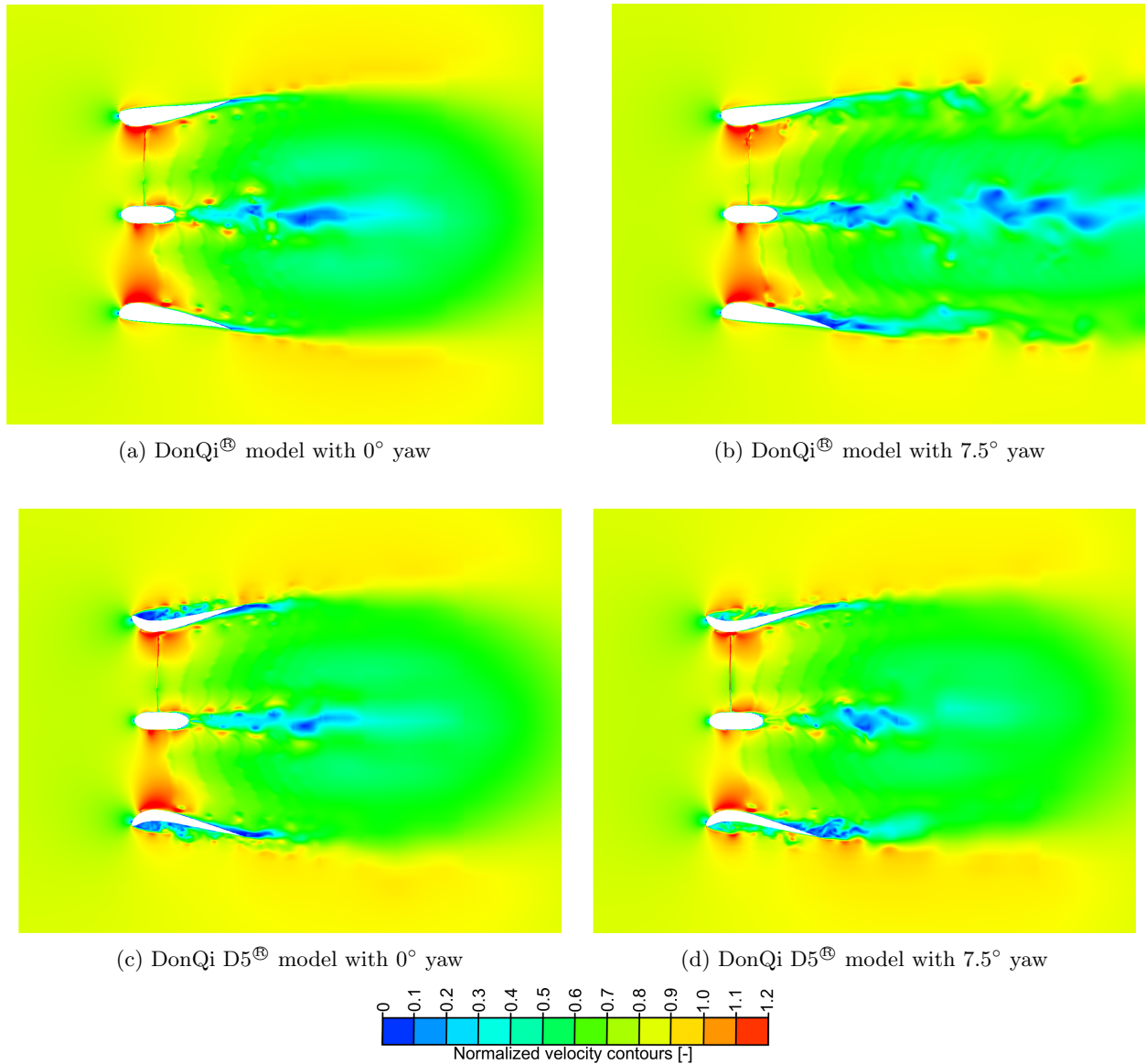
Figure 3: Velocity contours colored with normalized streamwise velocity.

American Institute of Aeronautics and Astronautics

B. Aerodynamic performance

The pressure coefficient c_p distribution over the duct chord length c is shown in Figure 4 (a) and (b). The values are obtained as time average over two complete turbine rotations after reaching temporal convergence. The negative (suction) side corresponds to the inside of the duct and the positive (pressure) side to the outside of the duct. The integral of pressure coefficient curve for the DonQi D5® model returns a larger thrust force coefficient in comparison to the DonQi® model, both in non-yawed and yawed inflow conditions. The axial thrust force generated by the duct has a direct consequence on the velocity at the turbine plane and ultimately the performance of the DWT model.[6]

Table 2 gives a succinct summary of the aerodynamic performance coefficients of the two DWT models under different inflow conditions. The duct thrust coefficient C_{TD} and the turbine thrust force coefficient $C_{Tturbine}$ are defined as:

$$C_{TD} = \frac{T_D}{\frac{1}{2}\rho U_\infty^2 S_{turbine}}, \tag{5}$$

$$C_{Tturbine} = \frac{T_{turbine}}{\frac{1}{2}\rho U_\infty^2 S_{turbine}}, \tag{6}$$

where T_D is the duct thrust force generated by the duct surface, $T_{turbine}$ is the turbine thrust force generated by the turbine blades and $S_{turbine}$ is the turbine surface area equal to $\pi R_{turbine}^2$.

The power coefficient C_P, expressed as a function of turbine thrust force coefficient $C_{Tturbine}$ and the azimuthally averaged surface integral of the axial velocity distribution U_x/U_∞ along the turbine's plane of rotation is given by:

$$C_P = \frac{P}{\frac{1}{2}\rho U_\infty^3 S_{turbine}} = C_{Tturbine} \oint_{S_{turbine}} \frac{U_x}{U_\infty}. \tag{7}$$

Even if some researchers consider the duct exit area S_{exit} for C_{Pexit} calculations, in this study we use $S_{turbine}$. When using S_{exit} as reference area, the C_{Pexit} obtained is smaller than the C_P shown hereinafter.

(a) Non-yawed inflow.

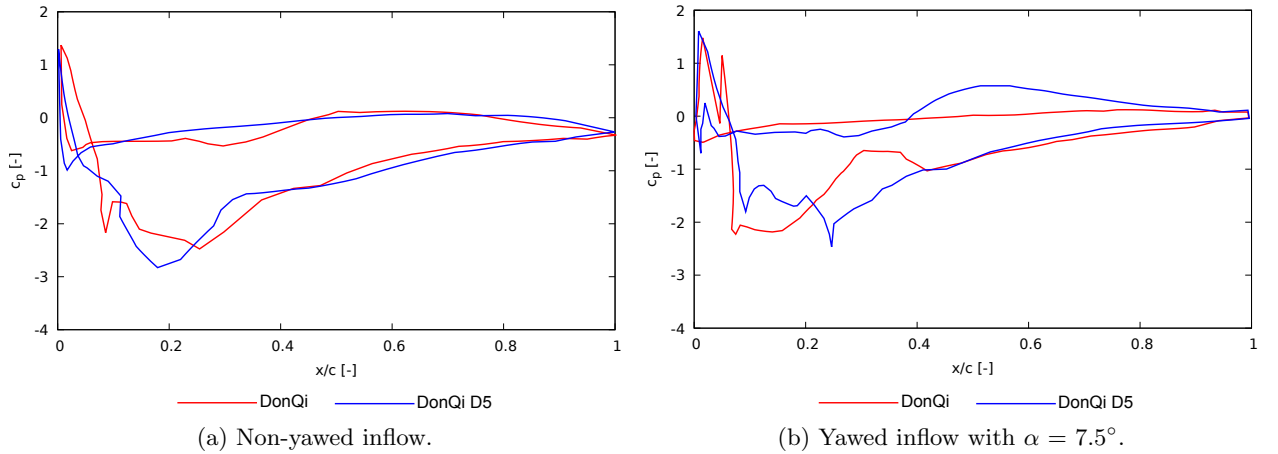(b) Yawed inflow with $\alpha = 7.5°$.

Figure 4: Time-averaged duct surface pressure coefficient in different inflow conditions.

Table 2: Aerodynamic performance coefficients for the two DWT models.

	DonQi		DonQi D5	
	0°	7.5°	0°	7.5°
C_{TD}	0.4238	0.3587	0.4812	0.5014
$C_{Tturbine}$	0.8292	0.7170	0.8417	0.8803
C_P	0.7545	0.6309	0.7675	0.7922

American Institute of Aeronautics and Astronautics

The comparison of the aerodynamic performance coefficients of the two DWT models in Table 2 shows that, for the same duct exit area, DonQi D5 model outperforms DonQi® model, both in non-yawed and yawed inflow conditions. The performance improvement for the DonQi D5 model can be attributed to the duct profile camber, which enhances C_{TD} and ultimately the C_P values.

For the DonQi® model at $\alpha = 7.5°$, C_{TD} returns a lower value in comparison to the C_{TD} at $\alpha = 0°$. As a consequence, $C_{Tturbine}$ and C_P calculated at $\alpha = 7.5°$ is lower by 13.5% and 16.4% respectively than that calculated at $\alpha = 0°$. Contrariwise, for the DonQi D5 model, C_{TD} at $\alpha = 7.5°$ is higher than that obtained at $\alpha = 0°$. As explained before, this is because the duct camber delays duct wall flow separation on the suction side in yawed inflow conditions (see Figure 3 (d)), thereby increasing the C_{TD} as also noted in 2D simulation by Dighe et al.[21] Then, the $C_{Tturbine}$ and C_P calculated at $\alpha = 7.5°$ is higher by 4.4% and 3.2% respectively than that calculated at $\alpha = 0°$ for the DonQi D5 model.
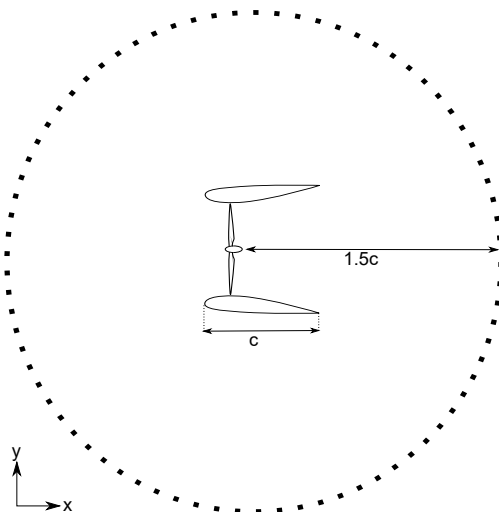
C.   Aeroacoustic performance

Figure 5: Schematic showing 72 microphones positioned at 1.5c from the center of the DWT and normal to the plane of turbine rotation

The effect of the duct geometry and inflow conditions on the aeroacoustic behavior of the two DWT models is investigated in this section. Noise is estimated on a circular array of 72 equally spaced microphones in the $x - y$ plane placed at 1.5c from the plane of rotation (Figure 5).

Figures 6 (a) and (b) shows the Overall Sound Pressure Level (OASPL) expressed in decibel (dB) with reference pressure equal to 20×10^{-6} Pa. Results are integrated from 2 Hz to 392.4 Hz, i.e. up to 20 times the Blade Passing Frequency (BPF). It can be observed that the OASPL generated by the DonQi D5 model is higher than that of the DonQi® one, both in non-yawed and yawed inflow conditions. Starting with the non-yawed inflow (Figure 6 (a)), differences in the OASPL directivity patterns are observed; they are localized in certain flow directions, i.e. in the axial direction upstream of the DWT and at $\pm 120°$. At these locations, the DonQi D5 model is approximately 15 dB and 20 dB louder than the DonQi® model. For the yawed inflow configuration (Figure 6 (b)), the directivity patterns are almost similar to the zero-yaw angle case but tilted. However, the difference in OASPL between the two configurations is smaller than at zero yaw-angle case, i.e. the DonQi D5 model is 8-10 dB louder than the DonQi® model.

The shape of the directivity plots for the DonQi D5 model, both in non-yawed and yawed inflow conditions, show the appearance of larger lobes in the downstream direction in comparison to the DonQi® model. This can be associated to turbulent boundary layer trailing edge noise caused by the turbulent flow structures convecting along the outer surface of the duct,[22] as shown previously in Figure 2. Noise increase in the axial direction is instead related to the variation of the local boundary layer thickness at the turbine plane, and due to the presence of an additional noise source related to flow instabilities, also found by Avallone et al.[22]
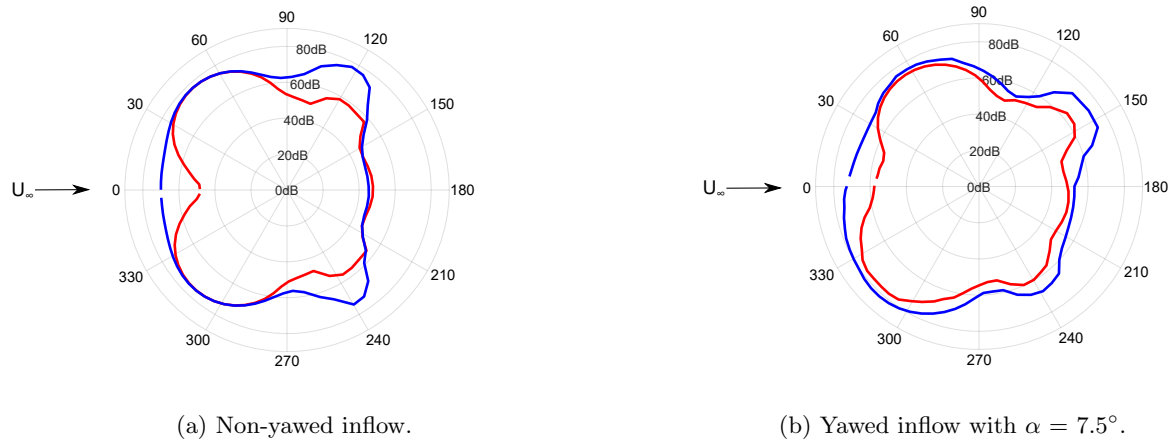
American Institute of Aeronautics and Astronautics

(a) Non-yawed inflow.

(b) Yawed inflow with $\alpha = 7.5°$.

Figure 6: Overall Sound Pressure Level (OASPL) obtained for the two DWT models in (a) non-yawed inflow condition and (b) yawed inflow condition.

IV.   Conclusions

The effects of yawed inflow on the aerodynamic and aeroacoustic performance of DWT are investigated using a computational approach. Lattice-Boltzmann Very-Large-Eddy Simulations are used. The following conclusions can be drawn:

- DWTs can demonstrate yaw insensitivity. The duct acts like the annular wing that sees the yaw angle as the increased angle of attack; the effect of which increases the duct thrust force coefficient and ultimately the power coefficient for the DWT model. The yaw insensitivity for the DWT model, however, strongly depends on the aerodynamic mutual interactions between the duct and turbine, which changes with the duct geometry, turbine configuration and yaw angle.

- The duct shape has a strong effect on the aeroacoustic performance of the DWT. An increase in duct cross-section camber increases the noise generated by the DWT model, both in non-yawed and yawed inflow conditions. The additional noise source results from the turbulent flow structures convecting along the surface of the duct.

Acknowledgments

References

[1] Gielen, D., et al. "The role of renewable energy in the global energy transformation." Energy Strategy Reviews, 2019

[2] van Bussel, G J W. "The science of making more torque from wind: Diffuser experiments and theory revisited." Journal of Physics: Conference Series. Vol. 75. No. 1. IOP Publishing, 2007.

[3] Stathopoulos, Ted, et al. "Urban wind energy: Some views on potential and challenges." Journal of Wind Engineering and Industrial Aerodynamics, 2018.

[4] Igra, O. "Research and development for shrouded wind turbines." Energy Conversion and Management, 1981.

[5] Phillips, D. G., et al. "CFD modelling and the development of the diffuser augmented wind turbine." Wind and Structures, 2002.

[6] Dighe V.V., et al. "Characterization of aerodynamic performance of ducted wind turbines: A numerical study." Wind Energy (in review).

[7] Avallone, F., et al., "On the Effect of the tip clearance on a diffuser-augmented wind turbine." Renewable Energy (in review).

[8] Anselmi, L. "Computational analysis of ducted wind turbines noise." Master thesis- TU Delft repository, 2017.

[9] Avallone, F., Casalino, D., & Ragni, D. (2019). On the Effect of the Tip Clearance on the Aerodynamic and Aeroacoustics of a Diffuser-Augmented Wind Turbine. In AIAA Scitech 2019 Forum (p. 1294).

[10]Avallone, F., Van der Velden, W. C. P., Ragni, D., & Casalino, D. (2018). Noise reduction mechanisms of sawtooth and combed-sawtooth trailing-edge serrations. Journal of Fluid Mechanics, 848, 560-591.

[11]Chen, S., & Doolen, G. D. (1998). Lattice Boltzmann method for fluid flows. Annual review of fluid mechanics, 30(1), 329-364.

[12]Succi, S. (2001). The lattice Boltzmann equation: for fluid dynamics and beyond. Oxford university press.

[13]Shan, X., Yuan, X. F., & Chen, H. (2006). Kinetic theory representation of hydrodynamics: a way beyond the NavierStokes equation. Journal of Fluid Mechanics, 550, 413-441.

[14]Teixeira, C. M. (1998). Incorporating turbulence models into the lattice-Boltzmann method. International Journal of Modern Physics C, 9(08), 1159-1175.

[15]Launder, B. E., & Sharma, B. I. (1974). Application of the energy-dissipation model of turbulence to the calculation of flow near a spinning disc. Letters in heat and mass transfer, 1(2), 131-137.

[16]Chen, S., & Doolen, G. D. (1998). Lattice Boltzmann method for fluid flows. Annual review of fluid mechanics, 30(1), 329-364.

[17]Ffowcs Williams, J. E., Dowling, A. P., & Goldstein, M. E. (1978). Sound production in a moving stream. Philosophical Transactions of the Royal Society of London. Series A, Mathematical and Physical Sciences, 288(1353), 321-349.

[18]Farassat, F., & Succi, G. P. (1980). A review of propeller discrete frequency noise prediction technology with emphasis on two current methods for time domain calculations. Journal of Sound and Vibration, 71(3), 399-419.

[19]Ten Hoopen, P. D. C. (2009). An experimental and computational investigation of a diffuser augmented wind turbine; with an application of vortex generators on the diffuser trailing edge.

[20]Jeong, J., & Hussain, F. (1995). On the identification of a vortex. Journal of fluid mechanics, 285, 69-94.

[21]Dighe, V., Suri, D., Avallone, F., & van Bussel, G.J.W: Ducted wind turbines in yawed flow: A numerical study, Wind Energ. Sci. Discuss., https://doi.org/10.5194/wes-2019-62, in review, 2019.

[22]Avallone, F., Casalino, D., Ragni, D. (2019). On the Effect of the Tip Clearance on the Aerodynamic and Aeroacoustics of a Diffuser-Augmented Wind Turbine. In AIAA Scitech 2019 Forum (p. 1294).